Synthesis of nanostructured Ti thin films by combining glancing angle deposition and magnetron sputtering: A joint experimental and modeling study

Dervaux, Jonathan; Moskovkin, Pavel; Cormier, P-A.; Douhéret, O.; Konstantinidis, Stephanos; Lazzaroni, Roberto; Lucas, Stéphane; Snyders, Rony

Published in:
Thin Solid Films

DOI:
10.1016/j.tsf.2017.06.006

Publication date:
2017

Document Version
Publisher's PDF, also known as Version of record

Thin Solid Films 636 (2017) 644–657

Contents lists available at ScienceDirect

Thin Solid Films

journal homepage: www.elsevier.com/locate/tsf

Synthesis of nanostructured Ti thin films by combining glancing angle deposition and magnetron sputtering: A joint experimental and modeling study

J. Dervaux [a,*], P.-A. Cormier [a], P. Moskovkin [b], O. Douheret [c,d], S. Konstantinidis [a], R. Lazzaroni [c,d], S. Lucas [b], R. Snyders [a,d]

[a] Chimie des Interactions Plasma-Surface, University of Mons (UMONS), 20 Place du Parc, 7000 Mons, Belgium
[b] PMR-LARN, University of Namur (UNamur), 61 rue de Bruxelles, 5000 Namur, Belgium
[c] Chimie des Matériaux Nouveaux, University of Mons (UMONS), 20 Place du Parc, 7000 Mons, Belgium
[d] Materia Nova Research Center, 1 Avenue Nicolas Copernic, 7000 Mons, Belgium

ARTICLE INFO

Article history:
Received 23 July 2016
Received in revised form 26 May 2017
Accepted 2 June 2017
Available online 03 June 2017

Keywords:
Monte Carlo simulation
Titanium
Thin films
Glancing angle deposition
Magnetron sputtering
Nanostructured films
Porosity

ABSTRACT

In this work, glancing angle deposition and magnetron sputtering are combined to synthesize nanostructured Ti films. Different type of microstructures (tilted columns, straight pillars, zigzags) are obtained as a function of the experimental conditions. As a support, kinetic Monte Carlo simulations are performed to understand the observed trends using the NASCAM (NAnoSCAle Modeling) code. The latter is used to simulate the growth of the films and to explain the effect on the obtained structures of experimental parameters such as the substrate temperature, the gas pressure as well as the substrate tilting and rotation speed. NASCAM enables quantitative prediction of the density, the surface roughness, and the column shape asymmetry. In addition, the effective porosity (ϕ_e) of the structures was evaluated from the simulation data for two molecules presenting different size (0.64 and 3.20 nm). The results show that ϕ_e decreases with the size of the adsorbed molecule, from above 50% for the small molecule to below 10% for the larger one. This is understood by considering the accessibility of the pore as a function of the size of the molecules. These data are correlated to experimental results obtained by transmission electron microscopy.

1. Introduction

The control of the morphology on the sub-micrometer scale and the porosity of thin films enables to tailor the film properties. In many devices pervasive in society, in technological advances such as energy generation and storage, optics and displays, microelectronics and information processing; the design and the fabrication of thin films have been central new opportunities for performance improvements [1].

In this context, the synthesis of columnar thin films is of great interest. GLancing Angle Deposition (GLAD) enables the growth of such films presenting unique nanostructures, e.g., nanostructured columnar architectures. These films are extremely porous with a high specific surface area (up to 100 m^2/g for TiO_2 [2]). They consist of isolated slanted columns, vertical pillars, zigzag or helicoidally structures [3]. More precisely, the open porosity (Φ_e), which is accessible by the surrounding medium, can be tuned using the GLAD parameters, leading to a controllable specific surface area [4].

In this context, we have recently demonstrated that Magnetron Sputtering (MS) and GLAD can be successfully combined to tailor the structuration of the TiO_2 thin films at the nanoscale [5]. The combination of MS and GLAD benefits from the advantages of both methods to grow nanostructured thin films with a well-defined chemistry and crystalline constitution. Nevertheless, the relationship between the experimental parameters and the properties of the films are most of the time complex which makes the interpretation of the results and the prediction of the structure difficult.

In order to gain understanding on the fundamental mechanisms involved into the growth process the NASCAM (NAnoSCAle Modeling) code is used to simulate the film formation [6,7]. This code is based on a kinetic Monte Carlo (kMC) approach that can be used to model, at the atomic level, different processes such as film nucleation, film growth and post deposition modifications (i.e. annealing). It has already been successfully used to predict the morphology of amorphous silicon porous structures deposited at oblique angles [8]. The microstructure of

* Corresponding author.
E-mail addresses: Jonathan.Dervaux@umons.ac.be (J. Dervaux), Pierre-Antoine.Cormier@umons.ac.be (P.-A. Cormier), pavel.moskovkim@fundp.ac.be (P. Moskovkin), Olivier.Douheret@materianova.be (O. Douheret), Sephanos.Konstantinidis@umons.ac.be (S. Konstantinidis), Roberto.Lazzaroni@umons.ac.be (R. Lazzaroni), stephane.lucas@unamur.be (S. Lucas), Rony.Snyders@umons.ac.be (R. Snyders).

http://dx.doi.org/10.1016/j.tsf.2017.06.006
0040-6090/

Ti thin films synthesized by combining MS and GLAD is compared to the NASCAM simulation outputs using the same deposition and substrate movement parameters. The effects of these parameters on the thin film morphology are then discussed. These finding are applied to the experimental development of porous Ti thin films for which a complete study of the porosity is performed.

2. Materials and methods

2.1. Experimental details

All experiments were carried out in a cylindrical stainless steel chamber (height: 60 cm, diameter: 42 cm) evacuated by a turbomolecular pump (Edwards nEXT400D 160W) backed by a dry primary pump, down to a residual pressure of 6×10^{-4} Pa. The magnetron cathode with an unbalanced configuration of magnetic field was installed at the top of the chamber. Silicon wafer substrates (2 × 2 cm) were installed at a distance of 80 mm. A 2-in. in diameter and 0.25-in. thick Ti target (99.99% purity) was sputtered in DC mode in Argon atmosphere (12 sccm). The GLAD system allows the substrate tilting with an angle α and to rotate it (angle φ) either step by step or with a continuous angular speed (φ_s) as represented in Fig. 1. The α and the φ angle was varied in order to obtain different columnar morphologies. Zigzag structures were obtained by discrete rotations ($\varphi = +180°$ or $-180°$) while vertical pillars and helicoidal structures were generated by continuous rotation ($\varphi_s = 0.1$, 1.0 and 10.0°/s).

The deposition rate was ~10 nm/min using the following conditions: pressure = 0.13 Pa, target power = 150 W and $\alpha = 85°$. The film thickness was determined by a Dektak 150 profilometer and was kept constant for a given experimental series. The microstructure was characterized by field emission gun scanning electron microscopy (FEG-SEM Hitachi SU8020) and the nanostructure was investigated by transmission electron microscopy (TEM Philips CM200). The film roughness was evaluated by Atomic Force Microscopy (AFM) measurements, which were carried out in tapping mode with a Multimode 8 Bruker microscope equipped with a Nanoscope V controller and using etched Si tip probes (Ref. PPP-NCHR, Nanosensors, GmbH), ensuring sub-10 nm spatial resolution. The root mean squared roughness (R_{RMS}) was measured on a 5 × 5 μm surface area of the Ti film. The specific surface area was evaluated by krypton adsorption at 78 K using a volumetric adsorption apparatus (Triflex, Micromeritics). In order to obtain enough adsorption, 5 × 5 cm^2 films deposited on Si wafers were prepared for the measurements. They were divided into four pieces (2 × 2 cm^2) and degassed at 473 K for 5 h under vacuum at pressures of <1 mPa to remove any physically adsorbed species before performing the adsorption measurements.

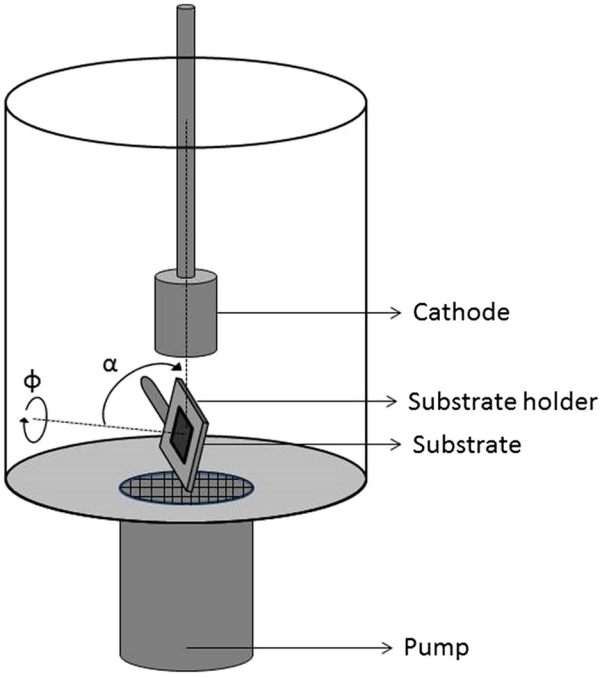

Fig. 1. Scheme of the deposition chamber.

2.2. Simulation protocol

The simulation of film growth on timescales of seconds or minutes is possible with kinetic Monte Carlo (kMC) algorithms [9,10]. This approach can be used for the modeling of various processes occurring at the surface such as the nucleation, growth, post deposition structural modification of the films or dynamic evolution of obliquely-deposited columnar structures [11,12]. These features are implemented into the NASCAM code which is freely distributed [6,7]. A particular feature of NASCAM is that the substrate can be displaced by translation, rotation or oscillation during the calculations, which is particularly suitable to simulate GLAD processes. A porosity evaluation plugin is also available [8].

The ballistic deposition approximation, which minimizes the computation time, represents the incoming vapor flux by a large number of hard spheres. Those particles travel along linear trajectories toward the substrate by reproducing the energy and angular distribution of the vapor source. The deposited particles become a part of the growing film.

The kinetic energy and the angular distribution of the incident particles are calculated by SRIM [13] and SIMTRA [14], respectively. SRIM is first used to calculate the energy and the direction of the particles that are sputtered away from the target. The transport of these species toward the substrate is then handled by the SIMTRA code, taking into account all collisions taking place in the gas phase. As a result, the angular and the energy distributions of the species involved in the film growth are generated and are then used as inputs in the NASCAM code. Finally, the porosity of the simulated films was characterized by the PoreSTAT software, from the NASCAM files [8].

The energy and the angular distribution of the species at the substrate location are derived for each working conditions by the introduction of the experimental parameters such as the working pressure, the power applied to the target, the racetrack size, the target-to-substrate distance, … Other parameters can be tuned by the NASCAM input file such as the number of deposited atoms (N) and the substrate size (XYZ) in order to compare simulated and experimental thin films having the same thickness. For direct comparison of the cross-sectional film morphology, 2D NASCAM simulations were performed while for the roughness, density and porosity evaluation, 3D simulations were performed. The deposition rate was fixed at 0.5 monolayer by second (0.16 nm/s), which is close to the experimental value (0.17 nm/s for Ti).

3. Results and discussion

3.1. Effect of deposition parameters on the thin film morphology

3.1.1. Angle of deposition (α)

The angle of deposition (α) is one of the most important parameter when synthesizing nanostructured thin films by using GLAD. For this set of experiments, all films were deposited at high power and low pressure: 150 W and 0.13 Pa, respectively. This power was chosen to maximize the deposition rate: 10 nm/min for $\alpha = 85°$ as an example. The film thickness was 500 ± 50 nm. Fig. 2 shows Ti thin films synthetized for various α angles from normal incidence ($\alpha = 0°$) to grazing angle ($\alpha = 89°$) with the corresponding kMC simulations obtained by using the NASCAM code. As input parameters, we have utilized the defined experimental parameters (150 W, 0.13 Pa). A number of 1.2×10^5 atoms was chosen to obtain a similar film thickness than the

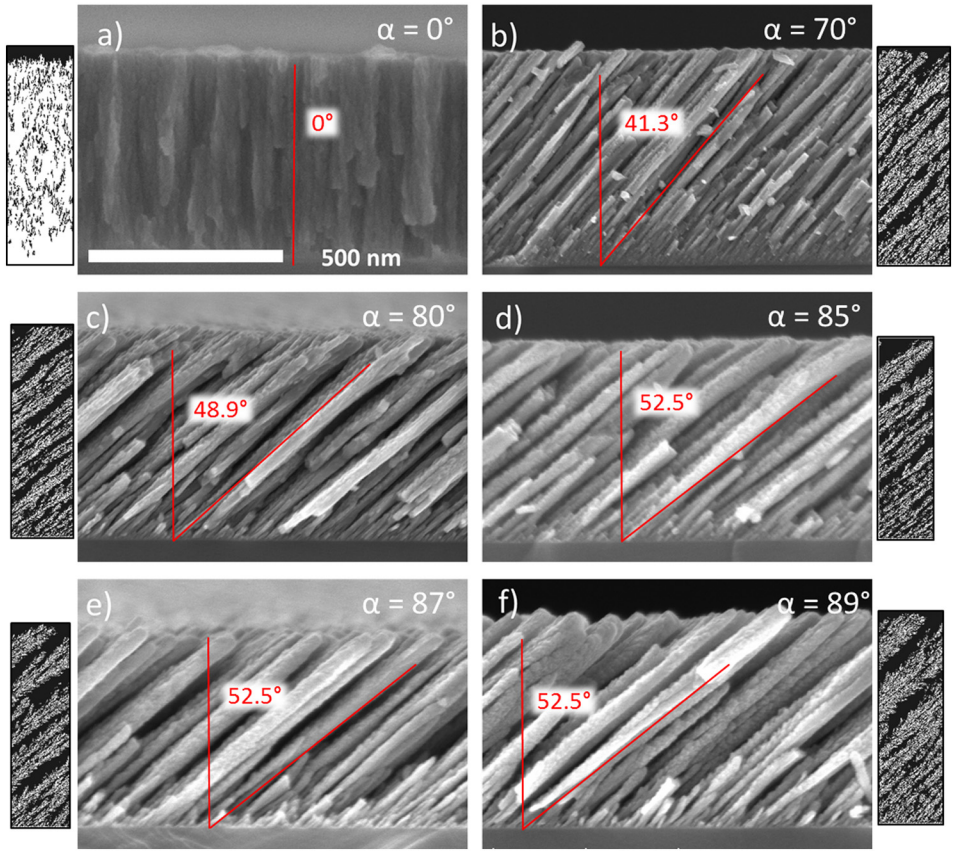

Fig. 2. Ti thin films synthesized at 150 W, 0.13 Pa for various angle of deposition (α) a) 0°, b) 70°, c) 80° d) 85°, e) 87 and f) 89° and the corresponding simulations. The red angle is the average columnar tilt angle (β) estimated by over 20 columns. (For interpretation of the references to color in this figure legend, the reader is referred to the web version of this article.)

one corresponding to the experimental conditions according to the size of the simulation box (x = 250 and Y = 2 Ti atom unit).

The increase of α leads to the nanostructuration of the film in the form of highly porous thin film composed by well separated tilted columns. This result is in line with previously published works. For example, the ones of Sit et al. [15] and Li et al. [16] who have reported on the synthesis of Ti columnar structures by combining GLAD and magnetron sputtering for α = 80° and 83°, respectively. The observed columnar structure is strongly influenced by atomic shadowing effects. In particular, at extremely oblique incidence angles of the flux (>70°) (measured relative to the substrate normal), the shadowing mechanism is strongly enhanced and results in a porous microstructure composed by columns inclined toward the vapor source [17]. The columnar tilt angle (β) and the inter columnar space drastically increase with α up to 70°. However, the film morphology does not change anymore for α > 85°. The columnar tilt angle (β) for α = 70° and 80°, measured from an average of 20 columns, increases from β = 41.3 ± 1.1° to 48.9 ± 1.5° an it stabilizes for α = 85° at ~52.5° ± 1.7° in line with the simulation data (Fig. 3). Based on these first data, it is obvious that the simulation methodology is perfectly adapted to our deposition process in view of the very good agreement between the measured and calculated β values.

The lower β value in comparison to the angle of deposition (α) is due to the parallel momentum conservation [17]. When the direction of vapor incidence is normal to the film surface, the diffusion during the accommodation of the adatoms is a few atomic distances in isotropic direction. However, under oblique incidence, the diffusion is in the same direction of the sputtered vapor beam. The amount of kinetic energy (momentum) preserved in the direction parallel to the film surface is only determined by the angle of incidence. This effect explains the variation of β as a function of α and of the kinetic energy of the impinging vapor atoms.

It has to be noted that since the substrate to target distance (8 cm) is not very high in our geometry, the diameter of the target (5 cm) have to be taken into account to distinguish the tilt angle of the substrate and the incident angle of the particles, since the majority of the latter comes from the racetrack region of the target (Fig. 4). The size of the particle source induces an angle of deviation in the α direction or in the φ direction (orthogonal to α) which increases with the target diameter.

Considering the geometry used of this work, the width of the sputter flux distribution at 0.13 Pa was determined by using the Monte Carlo

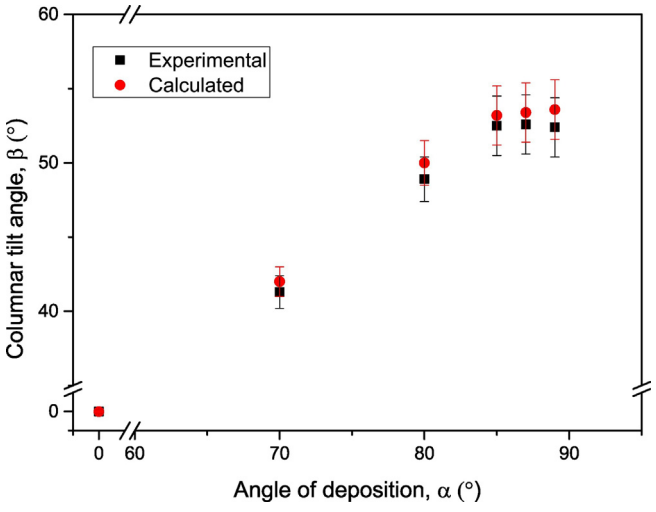

Fig. 3. The columnar tilt angle (β) as a function of the angle of deposition (α). The error bars were estimated by taking the tilt average over 20 columns.

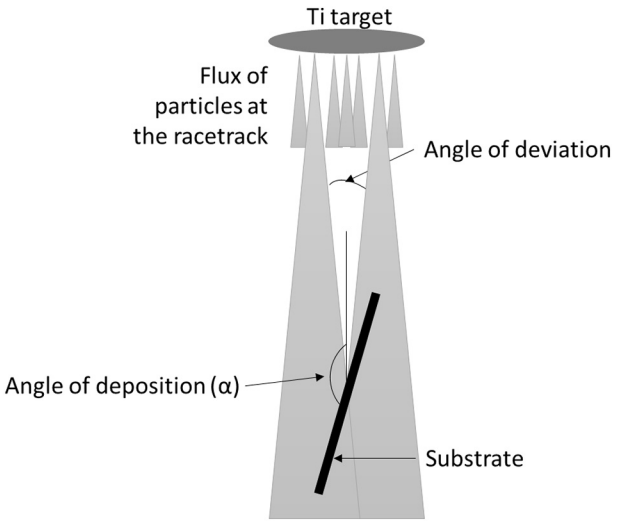

Fig. 4. Angle of deviation for sputtered particles in MS-GLAD configuration.

sputter flux transport simulator SIMTRA [14]. The angle of deviation is around 10°, depending on the angle of deposition (Fig. 5). This value is in line with other works for similar sputtering conditions [15,18]. The slight increase of the deviation angle with the angle of deposition is due to the geometrical inclination of the substrate leading to an asymmetric deposition. Indeed, the particles sputtered at the left side of the target have a higher probability to reach the left side of the substrate and inversely for the right side. This increase the deviation angle and can explain the similar morphologies for coatings synthesized for $\alpha = 85°$ and 89°.

As an output of this study, $\alpha = 85°$ was chosen for all further thin films synthesis because this angle allows a well-defined columnar structure obtained for reasonable deposition rate (10 nm/min).

3.1.2. Working pressure

Another important parameter in GLAD experiments is the working pressure. In "conventional" GLAD, the source material is usually thermally vaporized, most often by using a resistive heating system (thermal evaporation) or by high-energy electron beam bombardment (e-beam evaporation) [19,20]. Evaporation is typically performed in a high-vacuum environment, with gas pressures in the 10^{-4} to 10^{-8} Pa range. These low-pressure conditions limit the collisions between the

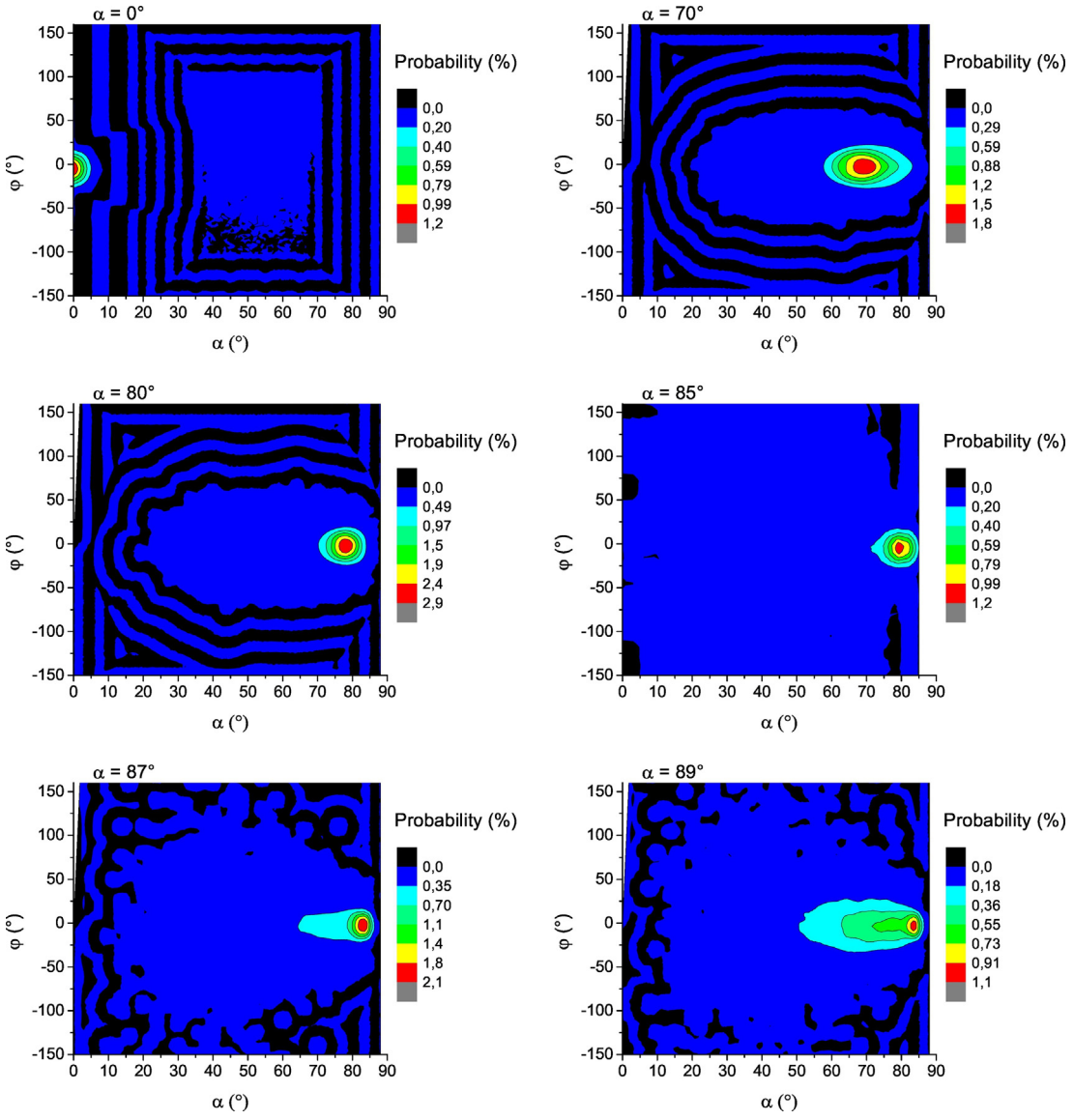

Fig. 5. Angle distribution of particles reaching the substrate deposited at 0.13 Pa and 150 W calculated by SIMTRA for various angle of deposition $\alpha = 0, 70, 80, 85, 87, 89°$.

vapor particles during their travel to the substrate ensuring a highly directional and collimated vapor flux that enhances the geometric shadowing effect and leads to porous nanostructures.

In this work, the working pressure was varied from 0.13 Pa to 1.3 Pa where 0.13 Pa corresponds to the minimum value necessary to maintain the magnetron discharge. The sputtering power and α were fixed at 150 W and 85°, respectively. The film thickness was 175 ± 20 nm. From the data presented on Fig. 6, we can see that β rapidly decreases as the sputtering pressure increases; from β = 52.7 ± 2.0° for 0.13 Pa to β = 13.8 ± 1.9° for 1.3 Pa. The modification of the columnar tilt angle could be attributed to a decrease of the collimation of the incident particle flux due to the increase of the collision probability as the pressure increases. Indeed, this probability mainly depends on the mean free path of the sputtered Ti atoms (λ_{Ti}) which is inversely proportional to the sputtering pressure following this equation (Eq. 1).

$$\lambda = \frac{k_B T}{\sqrt{2}\pi d^2 p} \quad (1)$$

where k_B is the Boltzmann constant, T is the temperature in Kelvin, p is pressure in Pascal, and d is the diameter of the gas particles in meters [21]. From this relation, λ_{Ti} (atomic diameter = 1.4 Å) ranges from 45 cm to 4.5 cm between 0.13 Pa and 1.3 Pa, respectively. These values are consistent with the mean free path determined for a gas mixture of Ar and Ti in similar pressure conditions: 50 and 5 cm at 0.15 and 1.5 Pa, respectively [22]. Considering the target to substrate distance (8 cm) that is used, an increase of the pressure induces a large amount of collisions between particles for the 1.3 Pa conditions resulting in a less porous films.

Fig. 7 shows the result of the kMC simulation for the synthesis of thin film at various pressures, from 0.13 to 1.3 Pa. The input parameters correspond to the experimental parameters used to synthesize the film presented on Fig. 6 (150 W, 85°). A number of 6×10^5 atoms was chosen to obtain a similar film thickness than the one corresponding to the experimental conditions according the size of the simulation box (x = 1000 and Y = 2 Ti atom unit).

The morphology of the simulated films is again in very good agreement with the experimental ones. Comparison of β values between experiments and simulations for films deposited at different sputtering pressures is shown in Fig. 8. Error bars were evaluated from an average of 20 measurements of β. In addition, the calculated λ_{Ti} as a function of the pressure is also presented. It appears that λ_{Ti} becomes lower than the target to substrate distance for pressure value < 0.7 Pa. In these conditions, very few collisions occur through the vapor phase.

The hypothesis of the effect of the mean free path on the film morphology is supported by the SIMTRA calculations which show that the mean number of collisions between particles increases from 0.7 to 25 when increasing the pressure from 0.13 to 1.3 Pa. This effectively confirms that for high pressure, the flux of sputtered Ti atoms is no longer collimated and the atoms land on the substrate with a quasi-random incident angle, which strongly reduces the shadowing effect. On Fig. 9, this modification of trajectories is well represented by the angular distributions of the incoming Ti atoms at the substrate, calculated by SIMTRA for 0.13 and 1.3 Pa. For p = 0.13 Pa, the angle with the largest probability is close to α = 80° with a low standard deviation (<30°) while for p = 1.3 Pa, the incident angle probability distribution shows a broad maximum between α = 30° and 80° with a large deviation (>100°). In that condition, a random flux for which most of the atoms in the gaseous phase are thermalized with the background gas is generated and therefore reaches the substrate with an isotropic velocity distribution function, as already described [23].

The energy distribution is represented on Fig. 10 a) and b) for 0.13 and 1.3 Pa, respectively. The decrease of the mean kinetic energy values from 8.9 to 1.4 eV as calculated by SIMTRA illustrates the thermalization of the sputtered particles when the pressure increases from p = 0.13 to p = 1.3 Pa. These results are consistent with previous data reported for the sputtering of an Au and a Ti target in Ar atmosphere showing that the thermalization degree of sputtered atoms increases as the pressure increases [24,25].

NASCAM modeling supports these experimental findings: the corresponding simulations performed using the same deposition parameters reveal column tilt angles (β), close to the measured values. These observations demonstrate that the main processes defining the microstructure of these films are (i) the self-shadowing mechanisms at the surface and (ii) the collisional processes of the sputtered particles in the gas phase.

Therefore, the NASCAM code, combining the angular and energy distributions of the film-forming particles, can be used to predict the thin film morphology. The analysis of the predicted film morphology at different pressures also allows determining the range of pressure where a ballistic deposition process occurs which, in our case, is between 0.13 and 0.26 Pa.

3.1.3. Substrate temperature

Since the mobility of the adatoms is the key mechanism behind the shadowing effect, it is also crucial to investigate the effect of the substrate temperature (T_s) on the morphology of the deposited films. Indeed, by increasing T_s, we expect to activate some diffusion phenomenon that will strongly impact the final morphology of the films.

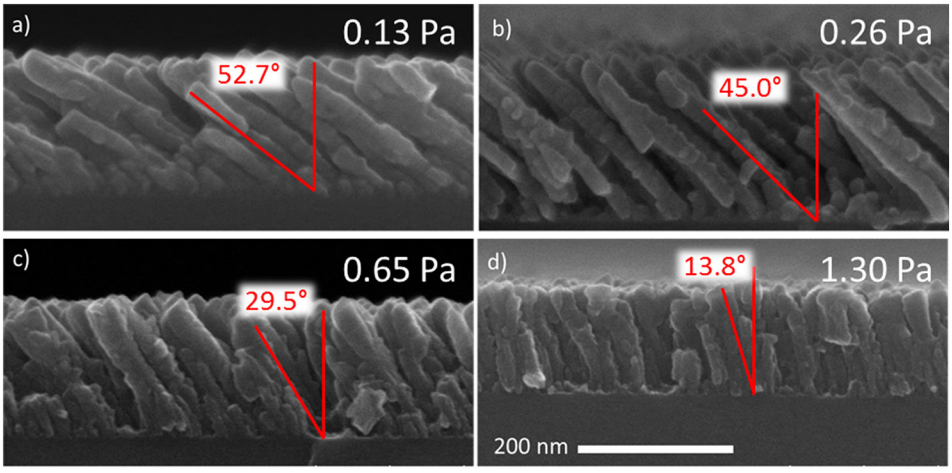

Fig. 6. Ti thin film synthesized at 150 W and 85° for various working pressure a) 0.13, b) 0.26, c) 0.65 and d) 1.30 Pa. The red angle is the average columnar tilt angle (β) estimated over 20 columns. (For interpretation of the references to color in this figure legend, the reader is referred to the web version of this article.)

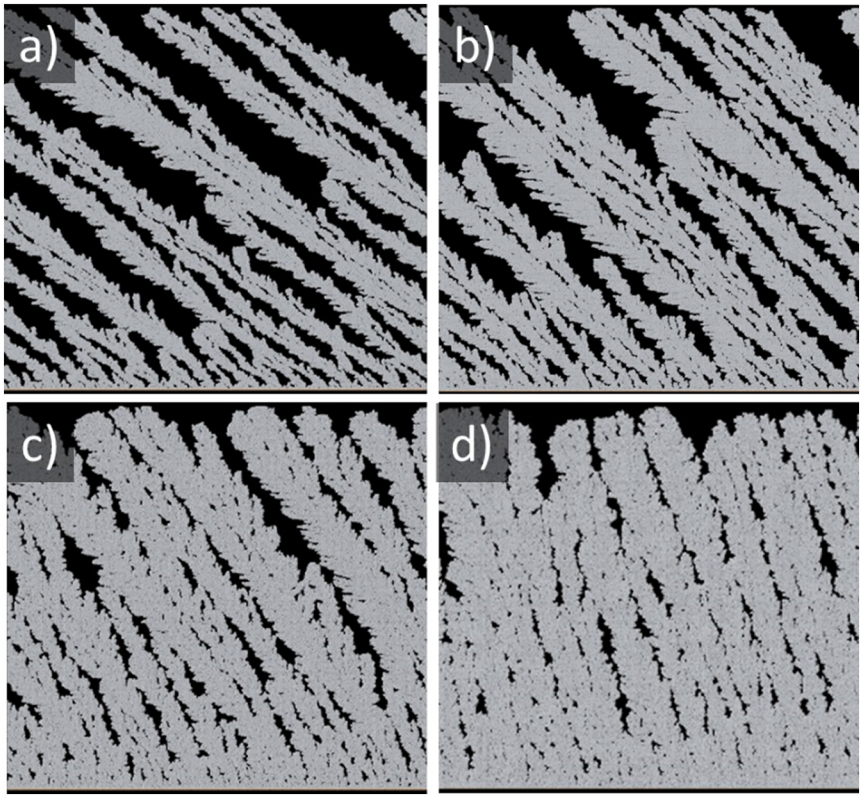

Fig. 7. Simulation data corresponding to Ti films synthesized at a) 0.13, b) 0.26, c) 0.65 and d) 1.30 Pa.

Tilted columnar Ti films were synthesized at different T_s ranging from 373 K to 873 K. 373 K corresponds to the temperature that is measured at the substrate surface without intentional heating. Such a temperature is reached because of the IR radiation emanating from the Ti target and other plasma-surface interaction phenomenon [26]. The film thickness was 225 ± 20 nm. Fig. 11 clearly demonstrates a decrease of β from 52.7 ± 1.8° to 41.2 ± 1.5° as T_s increases from 373 to 873 K.

These results could be understood according to structure zone models [27–30]. The earliest model, proposed by Movchan and Demchishin, describing vacuum-deposited materials, shows the development of different columnar morphologies as a function of the homologous temperature T_s/T_m where T_s is the substrate temperature and T_m is the melting point of the deposited material [31]. In this model, the Zone I regime, corresponding to $T_s/T_m < 0.3$, for which surface diffusion is limited, does not allow for the filling of the void regions that form in the microstructure because of the geometrical shadowing effect occurring during the GLAD experiments. In these conditions, the film growth proceeds by the formation of an underdense, fine nanofibrous microstructure that develops into a columnar morphology. The films synthesized for T_s up to 523 K belongs to this regime, with $T_s/T_m \sim 0.27$. In those conditions, for which geometric restrictions govern the formation of the microstructure, a strongly anisotropic deposition is observed, leading to a low influence of T_s on β.

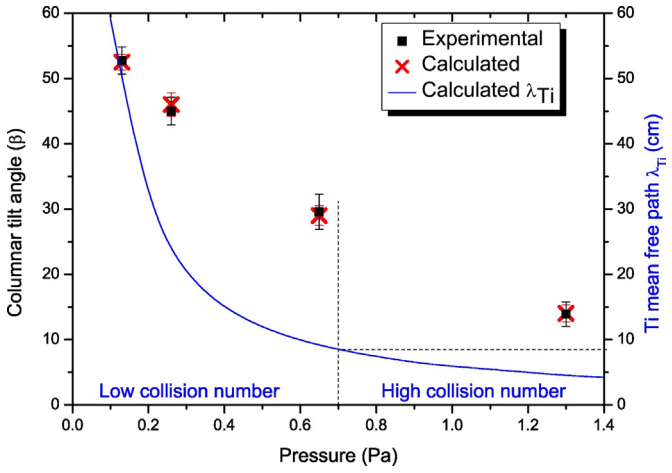

Fig. 8. Columnar tilt angle as a function of the working pressure for experimental and simulated thin films. The blue line corresponds to the evolution of the mean free path of the sputtered Ti atoms (λ_{Ti}) calculated from Eq. (1). (For interpretation of the references to color in this figure legend, the reader is referred to the web version of this article.)

It has to be noted that, for the "zone I" conditions of deposition (no intentional heating), the columnar tilt angle (β = 52.7 ± 2.1° in our case) is in line with the cosine rule (known as the Tait's rule) derived from geometric analysis of the inter-column shadowing geometry (Eq. (2)) [32].

$$\beta = \alpha - \arcsin\left[\frac{1-\cos\alpha}{2}\right] \quad (2)$$

Indeed, for these conditions, a good agreement is found between the experimental and calculated values. However, the measured columnar tilt angles are higher than the one obtained in previously reported works by Siad et al. and Alvarez et al. in similar conditions [25,33]. The higher sputtering power (350 W) to synthesize their Ti thin films could explain the difference of β. Indeed, Alvarez et al. showed that a dragging mechanism of the growing column surface can occur by a hyperthermal process promoting the growth of vertical columns. The incident flux of high energetic sputtered Ti atoms would mainly allow the horizontal displacement of adatom at the column surface and finally reduce the columnar tilt angle. In our case, the hyperthermal process was not observed as the measured β are similar to those observed in the case of GLAD thin films synthesized by thermal evaporation.

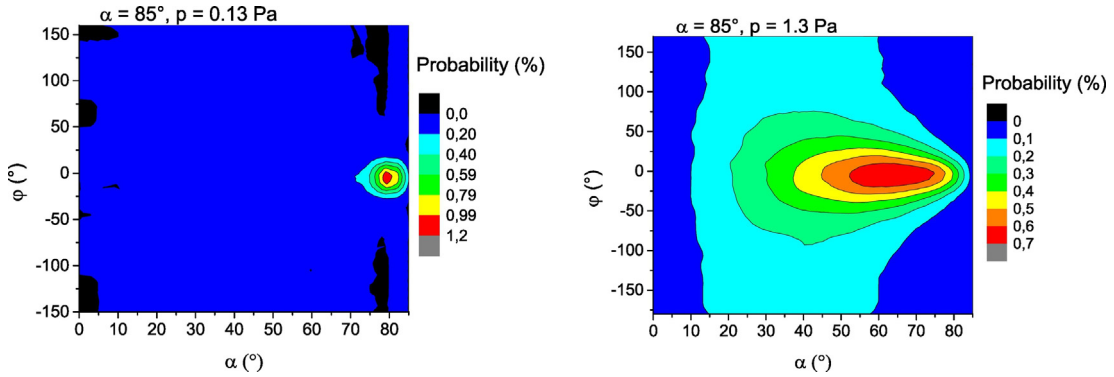

Fig. 9. Angular distribution of particles reaching the substrate for $\alpha = 85°$ calculated by SIMTRA for a working pressure of 0.13 and 1.3 Pa.

At higher T_s ($0.3 < T_s/T_m < 0.5$), the Zone II regime is reached, where surface diffusion has a dominant effect on the film growth. The resulting microstructure consists of tightly-packed columnar grains. The films synthesized between 723 K and 873 K correspond to T_s/T_m ratios of 0.37 and 0.45, respectively. T_s allows the activation of the diffusive surface transport leading to a decrease of the anisotropic character of the deposited film. As a consequence, β decreases.

Zone III ($T_s/T_m > 0.5$) corresponds to conditions for which bulk diffusion processes are activated, enabling grain boundary diffusion and recrystallization during growth. This regime has not been reached in our experimental window since such a kind of homologous temperature ($T_s > 973$ K for Ti) cannot be reached in our deposition set-up. Nevertheless, we expect that, in those conditions, the deposition would be almost isotropic even if the substrate is tilted. The columnar microstructure of the typical GLAD thin films would disappear, giving way to a dense film.

To simulate the growth at high temperature, the approximation of ballistic deposition has to be completed by diffusion phenomenon. There are several approaches for implementing the kMC simulation in this situation. The most accurate approach is the so-called "complete kMC" for which a table of all possible events associated to the physical mechanisms is created. It is the most time consuming method as it is necessary to calculate the rates for a huge number of events for all atoms. On the other hand, the "bond-counting" kMC method which is used in this work calculates the event rates taking into account the number of nearest neighbours of each atoms. In this specific event kMC, a predefined set of events is only allowed to occur for the atoms from the surface for example, and the rates of these events are used as inputs. Although the last approach is not as accurate as the "complete kMC" ones, it allows simulating the general behavior of the system and requires less computational time, making possible the simulation of the evolution of the system with a larger number of particles. This is important especially for the modeling of a system at elevated temperature since event rates increase according to an exponential law as a function of the temperature. The total number of steps required to model a system evolution during a given period of time increases in a similar way. Several physical mechanisms can be thermally activated (e.g. diffusion on substrate, hopping from substrate on an island, etc.). Event rates obey to an exponential law as the one described by Eq. (3):

$$w_i = w_0 \exp\left(\frac{-\Delta E_a}{k_B T}\right) \tag{3}$$

where w_0 is the attempt rate (it can be estimated as $w_0 = 2KT$), and ΔE_a is the activation energy for the event.

The activation energy of Ti self-diffusion ($E_{a,diff}$) obtained by radioactive tracers was reported to be 1.35 eV [34]. The energy of a hop up and a hop down from one atomic layer to another in diagonal ($E_{a\ up}$ and $E_{a\ down}$, respectively) were varied close to the $E_{a,diff}$ value. The values that lead to the better agreement with the experimental data, presented on Table 1, are 2.0 and 2.5 eV for $E_{a\ up}$ and $E_{a\ down}$, respectively, with $E_{a,diff}$ fixed at 1.35 eV. Finally, in the temperature and pressure ranges considered in this work, the probability that an evaporation event occurs is lower than for a diffusion event (the vapor pressure of Ti at 1783 K is 10^{-4} Pa [35]). The activation energy for Ti evaporation from the substrate or from the Ti film surface ($E_{a\ evap}$) was thus fixed at 5.0 eV, which is significantly higher than $E_{a,diff}$ (Table 1).

As already mentioned, the impact of diffusion phenomena on the film morphology increases as the substrate temperature (T_s) increases. In order to evaluate it, the growth of columnar titanium films was simulated at different T_s ranging from 373 K to 873 K, a range of temperature corresponding to our experimental conditions. Fig. 12 shows the corresponding simulations using the experimental conditions as input (150 W and 0.13 Pa). The agreement between the experimental data shown on Fig. 11 and the simulated data confirm that the diffusion

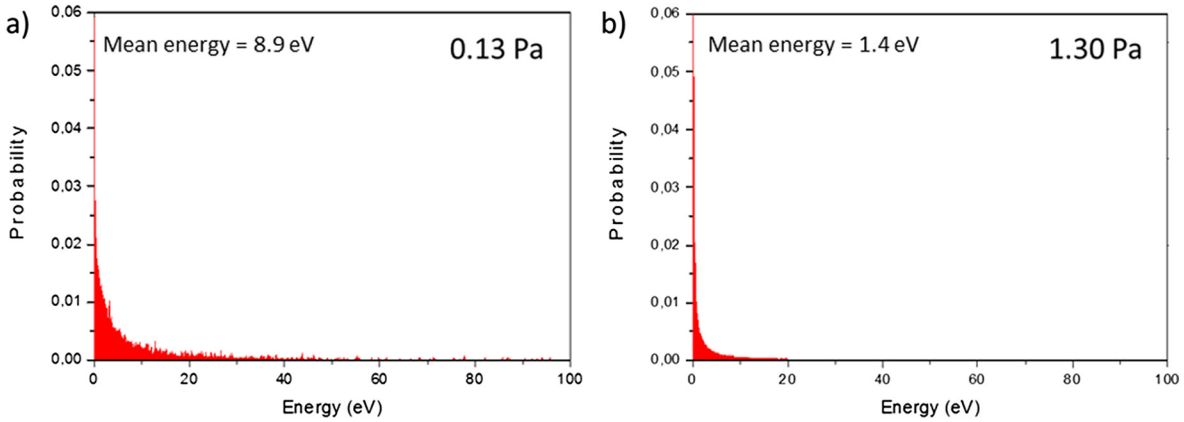

Fig. 10. Energy distribution of particles reaching the substrate calculated by SIMTRA for a power of 150 W and a working pressure of a) 0.13 and b) 1.3 Pa.

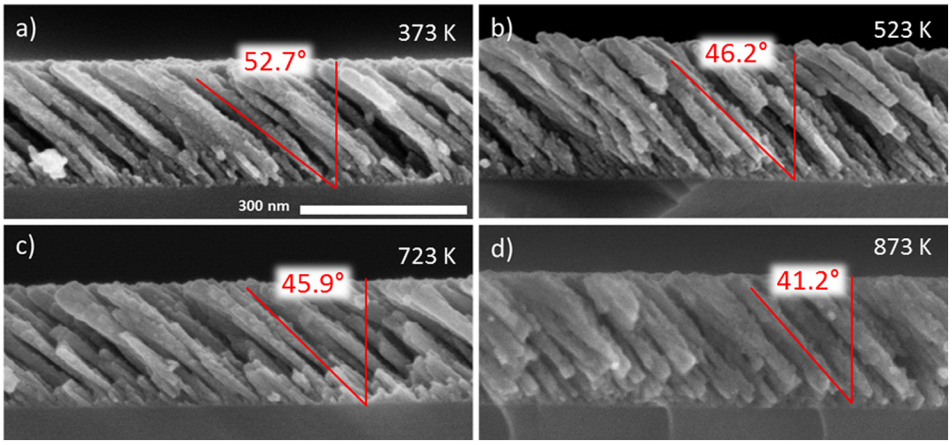

Fig. 11. Ti films synthesized at 0.13 Pa and 150 W for various T_s: a) 373, b) 523 c) 723 and d) 873 K. The red angle is the average columnar tilt angle (β) estimated over 20 columns. (For interpretation of the references to color in this figure legend, the reader is referred to the web version of this article.)

phenomenon is likely the reason for the evolution of β with T_s. Nevertheless, as well as T_s increases the deviation with the Tait's rule increases also showing the limit of this model exclusively based on geometrical principles (Fig. 12).

As previously saw, the parallel momentum affects β and this effect is enhanced by a high diffusion as, under oblique incidence, the diffusion is considerably larger. Two other key processes influence the surface diffusion of adatoms away from their initial impingement spot: (i) the surface contamination level and (ii) the self-diffusion distance [17].

(i) The presence of molecules from background gases in the system can influence the surface diffusion. Since the exact desorption energies of those molecules and the partial pressure of the background gases are unknown, the effect of contamination cannot be calculated directly. However, in our case, the Ti target was sputtered in pure argon enhancing the getter effect leading to a reduce contamination. Moreover, a constant residual pressure of 6×10^{-4} Pa was obtained before each deposition. The background gas conditions are thus similar between experiments.

(ii) After accommodation, the adatoms will start hopping over the surface until they are buried under newly arriving vapor atoms. The burial rate is defined as the rate at which the time between atomic layer formation (τ_m) (depending to the deposition rate) equals the mean time between two hops (τ_h) [17]. τ_h is determined by the film temperature (T), the energy needed for one hop (E_a) and the lattice vibration frequency (ω) is given by Eq. (4).

$$\tau_h = \frac{1}{\omega} \exp\left(\frac{E_a}{k\,T}\right) \tag{4}$$

Neglecting the influence of background gases, an average root means square (RMS) diffusion distance (Λ) can be calculated (Eq. (5)) where a_h is the distance of one absorption site [17]. Conversely to the parallel momentum, this diffusion has no directional component.

$$\Lambda = \frac{1}{2}\, a_h \sqrt{\frac{\tau_m}{\tau_h}} \tag{5}$$

From these considerations T_s and the activation energy seems to be the critical parameters. Moreover, the similar form of Eqs. 3 and 4 reveals that the simulations well traduce the diffusion of atoms at the surface. The influence of E_a for the different physical events on the film morphology has been investigated. The study has revealed that $E_{a\ up}$ and $E_{a\ down}$ are the critical diffusion event. Based on these results, the empirical model proposed by Movchan and Demchishin for thin film deposited at normal incidence ($\alpha = 0°$) can be adapted to oblique angle deposition at different T_s (Fig. 13).

Fig. 14 shows simulations carried out using the same experimental conditions (150 W, 0.13 Pa, 373 K), with and without diffusion. The similar columnar tilt angle for both simulations ($\beta = 52.7 \pm 2.1°$) demonstrates that ballistic deposition is a good approximation when working in "zone I" of the structure zone model. It appears that, for low T_s, negligible surface diffusion is allowed since β is the same for both the simulations. In this case, the energy brought to the growing film is too low in comparison with $E_{a,diff}$. However, for higher T_s, the self-diffusion starts to affect the film morphology and lower β values are calculated. It is explained by considering the effect of the surface diffusion of Ti adatoms and especially by hops up from one level layer to another combined with the effect of the conservation of the parallel momentum. This combination leads to an anisotropic surface diffusion promoting the hops in the direction of incident particles and thus the decrease of β.

Table 1
Physical events with the corresponding activation energies used to simulate the growth of titanium thin films.

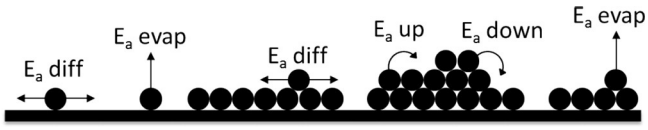

Physical events	Activation energies (eV)
E_a diff	1.35
E_a up	2.0
E_a down	2.5
E_a evap	5.0

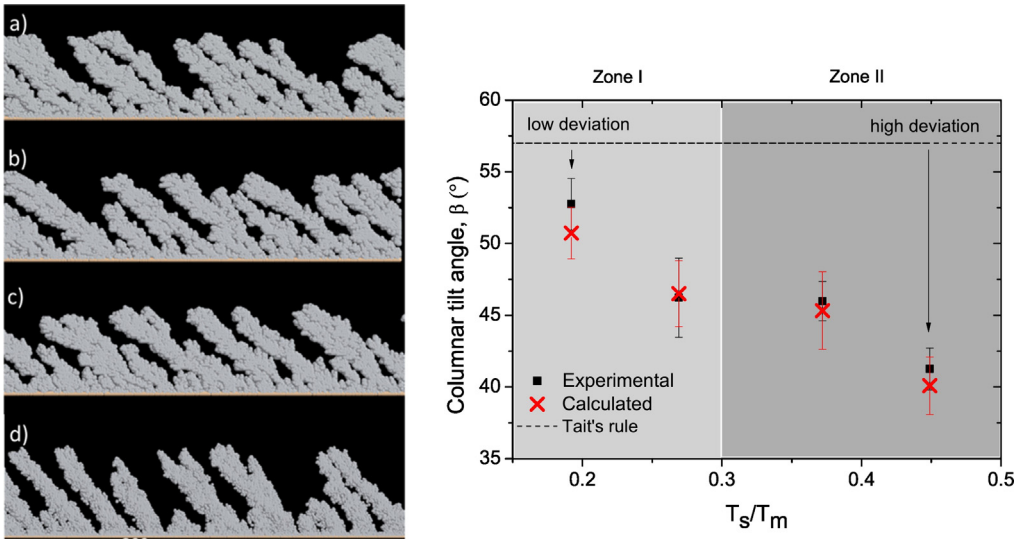

Fig. 12. Deposition of columnar thin films simulated at oblique angle ($\alpha = 85°$) for different Ts: a) 373 K, b) 523 K, c) 723 K and d) 873 K and the corresponding β from experiment and simulation as a function of the homologous temperature. The dashed line shows the value of β expected for the Tait's rule.

3.1.4. Substrate rotation

According to the previous data, the experimental conditions allowing for the growth of films presenting well defined columnar structures are: a low T_s (<523 K) and a low sputtering pressure (0.13 Pa). These conditions have therefore been used to study the effect of the rotation of the substrate on the film microstructure. The value of ϕ (the angle of rotation) significantly influences the microstructure of the films. For a discrete variation of ϕ (+180° or −180°), zigzag structures are obtained with different number of branches (Fig. 15 a, b, c) while for a continuous rotation of the substrate (0.1, 1.0 and 10.0°/s), vertical pillars or helicoidal structures are generated (Fig. 15d, e, f). The film thickness was 350 ± 20 nm.

We observe that, in the initial stages, the films are composed by a larger number of small columns. With the onset of competitive growth, the number of columns rapidly decreases when the film becomes thicker. Even if extinct columns can also be observed for the slanted columnar morphology (without ϕ variation), this effect is enhanced by the changing of the substrate orientation. The latter also induces a β variation in the zigzag microstructure (Fig. 15a). It is related to the change in the local deposition geometry generated when the substrate is rotated in ϕ. The initial column arm is deposited onto a flat substrate with a uniform α leading to a columnar tilt angle. After the first columnar arm of the zigzag is deposited and the substrate is rotated at 180°, the incident vapor encounters the surface with a different orientation. Indeed,

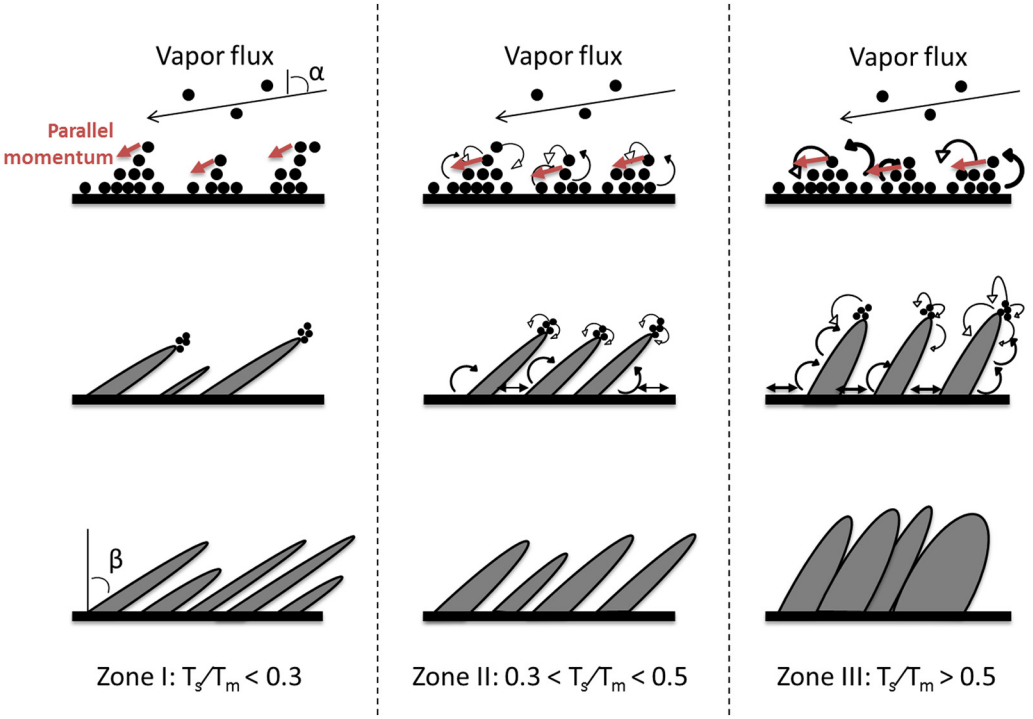

Fig. 13. Growth models expected for oblique angle deposition at different substrate temperature.

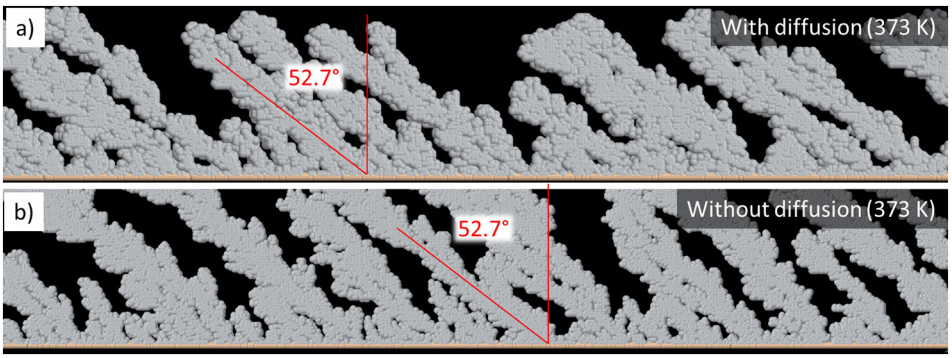

Fig. 14. Simulations (150 W, 0.13 Pa and 373 K) carried a) with diffusion and b) without diffusion. The red angle is the average columnar tilt angle (β) estimated over 20 columns. (For interpretation of the references to color in this figure legend, the reader is referred to the web version of this article.)

the deposition is now performed onto the column sidewall near the apex. When depositing at α onto a column tilted at β, the effective local deposition angle is $\alpha' = \alpha + \beta - 90°$ [19].

Modeling ballistic deposition without diffusion is considered for this section in order to keep the computational effort to a reasonable level. Fig. 16 shows the simulated data corresponding to films grown by varying the ϕ angle. The corresponding experimental data are presented on Fig. 15. The exacerbated competitive growth mode experimentally observed is also observed by simulation. It is caused by the change of the substrate orientation at oblique deposition angle which results in strong atomic shadowing and favors the growth of larger columns at the expense of smaller ones that die out. The inter-column competition starts during the nucleation stage [36]. In fact, when viewed at different stages of growth, the competition-driven evolution of the columnar growth generates a film morphology which is remarkably scale-invariant. These observations as well as the β variation in the zigzag microstructure are reproduced by the NASCAM simulations in line with the experimental results.

3.2. Deposited films properties

3.2.1. Roughness

For many applications such as dye sensitized solar cells, energy storage, gas sensors, photocatalytic films, etc., the performances of devices are particularly determined by the nanostructuration of the materials at the interface between the film and the external medium. In this context, a description at the nanoscale of the surface is therefore fundamental. The AFM technique is particularly suited to meet this objective.

Fig. 17 shows $1 \times 1\ \mu m^2$ AFM topographic images of slanted columnar films presenting a thickness of a) 30 nm, b) 50 nm and b) 125 nm deposited at 150 W, 0.13 Pa, 85°. In the first step of the growth, numerous islands are dispersed on the substrate surface. Their accumulation

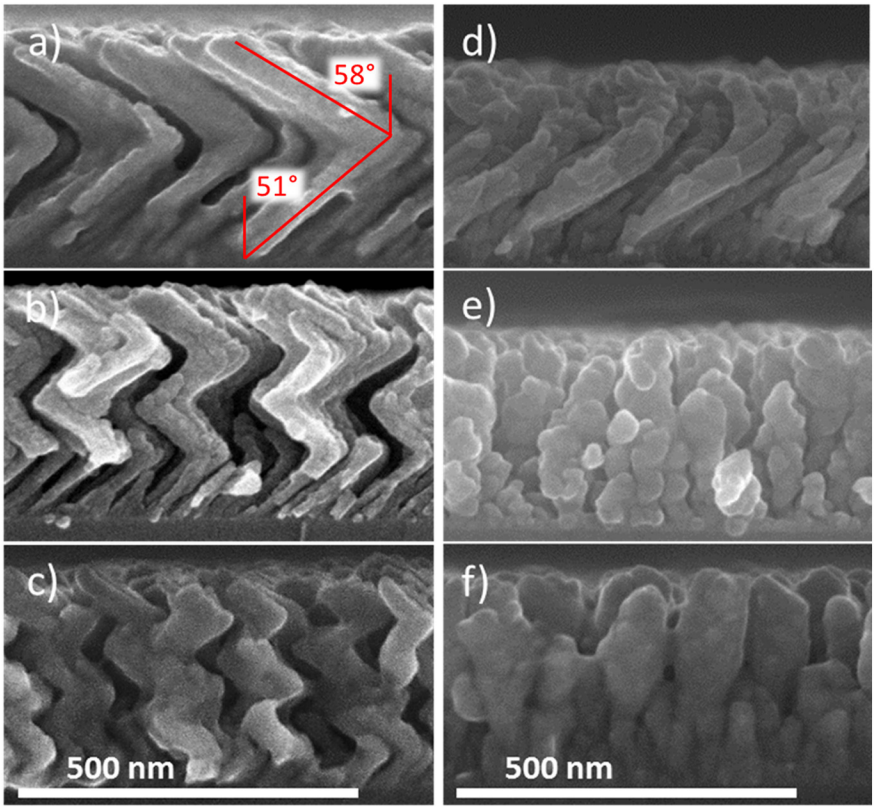

Fig. 15. Ti films (150 W, 0.13 Pa, 85°) deposited with various rotation movement of the substrate to generate a–c) zigzag structure d) at 0.1°/s helicoidal structures, e) 1.0°/s and f) 10.0°/s) vertical pillars.

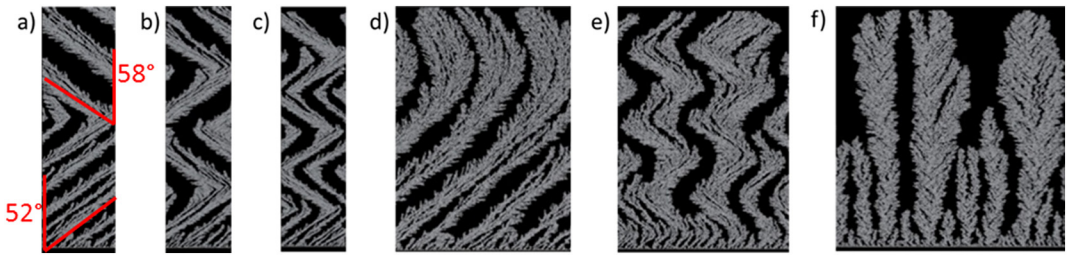

Fig. 16. Simulated Ti thin films deposited (a–c) with a discrete variation of φ (+180° or −180°) and (d–f) with a continuous rotation of the substrate (from 0.1 to 10°/s).

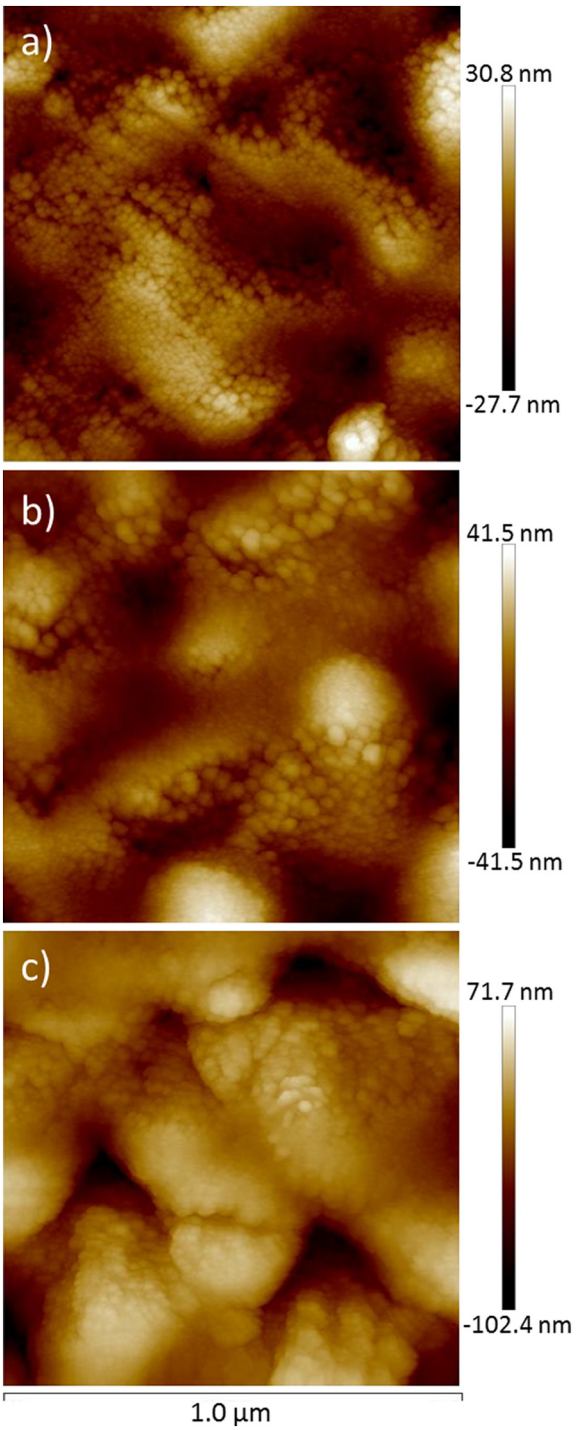

Fig. 17. 1 × 1 µm² AFM topographic images of slanted column films with a thickness of a) 30 nm b) 50 and b) 125 nm.

enhanced by the shadowing effect leads to the column formation. The column formation by merging of nucleation islands formed at the beginning of the thin film growth is well illustrated by the AFM topographic images.

Many experimental studies using AFM have shown that the film surface profile (i.e., the root-mean-square roughness of the column apexes) increases with thickness [20,37–39]. Fig. 18 shows the evolution of the experimental and calculated roughness (RMS) data, as obtained from NASCAM, as a function of the film thickness for slanted ($\alpha = 85°$) and vertically ($\alpha = 85°$ and $\phi = 10°/s$) oriented columnar structures. Roughness calculated from Nascam simulations is defined as arithmetic average of the absolute value of the surface height deviation: $w = \sqrt{h^2 - h2}$ where h is the local thickness of the film, and $\langle\,\rangle$ means the averaging over the whole film. In addition to the agreement between the two sets of data, these results show that the formation of the columnar structure is associated to the surface roughness. It appears that the roughness increases with the film thickness for both types of structures. Moreover, the results show that the roughness is also affected by the rotation of the φ angle, which leads to an increase of the competitive growth by merging and broadening of the columns. While the roughness reaches a plateau for the slanted columnar structures, it still increases with the thickness of the film. The broadening of vertically oriented columns has been also studied by experimental investigations, in line with basic models of ballistic deposition [40–42].

As the roughness increases quickly in the first steps of deposition, the density of the film dramatically decreases. The calculated density value is stable around 0.27 after the deposition of 10^6 atoms corresponding, in our case, to a thickness of 100 nm. This is calculated for the pillar structures and is also true for other structures such as slanted columns and zigzag. Even if knowing the density of the film provides indications about the film porosity, it cannot be used to predict the penetration of the molecules in the film.

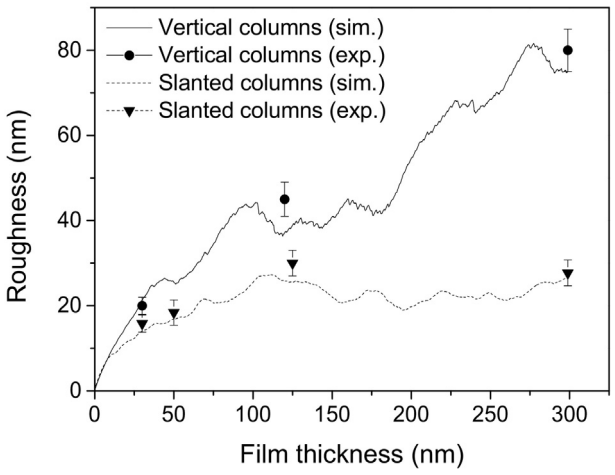

Fig. 18. Experimental (exp.) and calculated (sim.) roughness (RMS) evolution as a function of the film thickness for vertical and slanted column structures.

3.2.2. Porosity

If it is that TiO_2 is used for the design of dye-sensitized solar cells for example, the present work related to Ti films can be viewed as a first step toward the controlled synthesis of such films, since (i) the specific surface area that is exploited to adsorb the molecules mainly depends on the film morphology, and (ii) in a previous work, we reported similar TiO_2 thin film morphologies using the same experimental conditions [5]. The specific surface area of the films with a tilted columnar structure was evaluated experimentally to be 140 m^2/g by using Kr adsorption. Even if the value is in agreement with previbetous studies [4,43], the thin film geometry may perturb the measurements and calculating the porosity of the films from simulations could be useful. The open porosity, which defines the capacity to incorporate molecules or polymers, is a parameter of particular relevance in view of the potential applications of these porous coatings. The open porosity is defined as the ratio of the void volume in contact with the outer medium to the total volume of the film. Therefore, non-interconnected voids present in the solid phase do not contribute to the open porosity and belong to the so-called "closed porosity" (Fig. 19). When considering porosity, it is important to note that not all open pores can be used for molecule adsorption. Depending on the respective size of the pores and the molecules, some of them could be inaccessible, as illustrated on Fig. 19 for two molecules with different sizes. Therefore, the effective porosity (Φ_e) defines the fraction of the open porosity that is accessible by a molecule of a given size.

In order to evaluate Φ_e, the output of the NASCAM simulations has been analyzed using the PoreStat software [44]. The data have been treated for two spherical molecules (M1 and M2) having different diameters (M1 = 0.64 nm and M2 = 3.20 nm) to illustrate the dependence of Φ_e with the molecule size. To determine a representative Φ_e value, the size of the 3D simulation box must be large enough. The simulation box is defined by X (length), Y (width) and Z values (height) with the Ti covalent diameter (0.32 nm) as unit length. Preliminary results have shown that stable values are obtained for X ≥ 250 and Y ≥ 50. Z depends on the number of deposited atoms and the density of the film. To simulate a thin film with a thickness around 300 nm (X = 250 and Y = 50), the number of deposited atoms was fixed at 3.10^6. A 3D simulation of a synthesized film with substrate rotation (10°/s) mainly constituted by 4 pillars (highlighted by color lines) is shown in Fig. 20a and the corresponding representation of Φ_e in the case of the M2 molecule on Fig. 20b.

On Fig. 21, the evolution of Φ_e as a function of the experimental parameters (pressure, rotation motion) is presented for both molecules (M1 and M2). As expected, for all conditions a significantly better impregnation is obtained for the smallest molecule: around 50% for M1 vs. just above 5% for M2. This is explained by the nanoscale structure of the film. Fig. 22 compares a TEM image of a tilted Ti column synthesized without substrate heating (zone I) and a 2D simulation obtained in the same growth conditions (Fig. 22b). At the nanoscale, a hierarchical growth already reported in the case of pillar structures [45] is observed experimentally and expected from the simulation. It appears that individual columns present a substructure at the nanoscale. The hierarchical nature of the film growth leads to fractal geometries, where the microstructural details are similar when viewed at different length

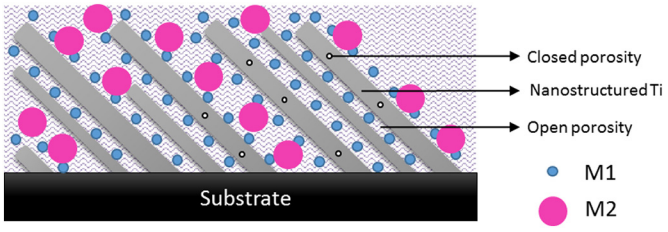

Fig. 19. Schematic representation of the open and closed porosity of a slanted columnar thin film impregnated by molecules with various sizes (M1 and M2).

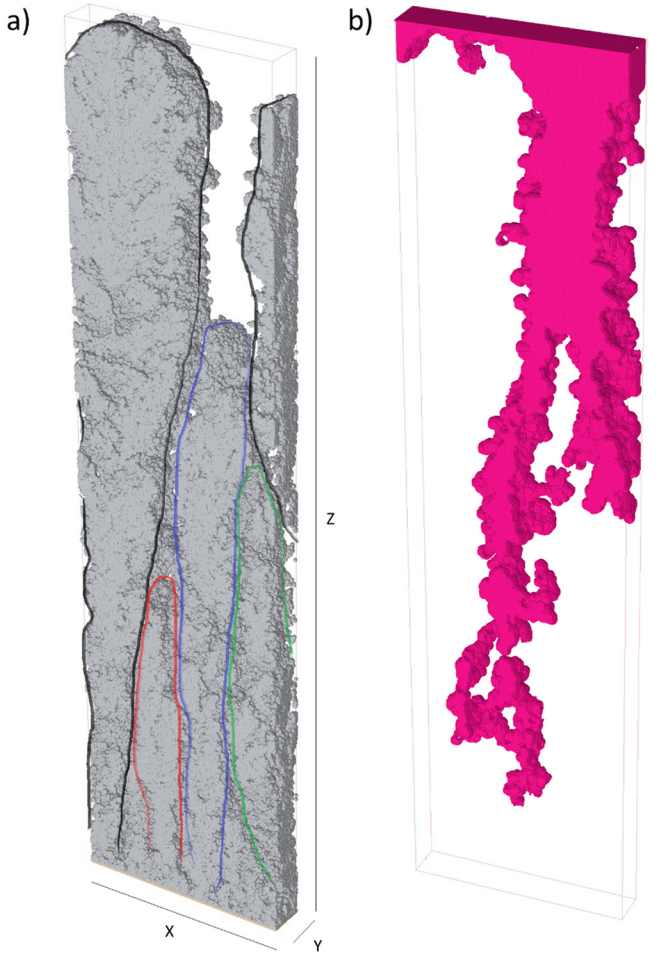

Fig. 20. Three-dimensional simulation of a porous Ti films mainly constituted by 4 pillars (highlighted by the color lines). The size of the object is for X = 250, Y = 50 and Z = 950 and it contains 3.10^6 deposited atoms. It corresponds to a film synthesized using a substrate rotation (10°/s) and a deposition angle of 85° (a). The corresponding representation of the effective porosity for a pore size ≥3.2 nm (M2) (b). (For interpretation of the references to color in this figure legend, the reader is referred to the web version of this article.)

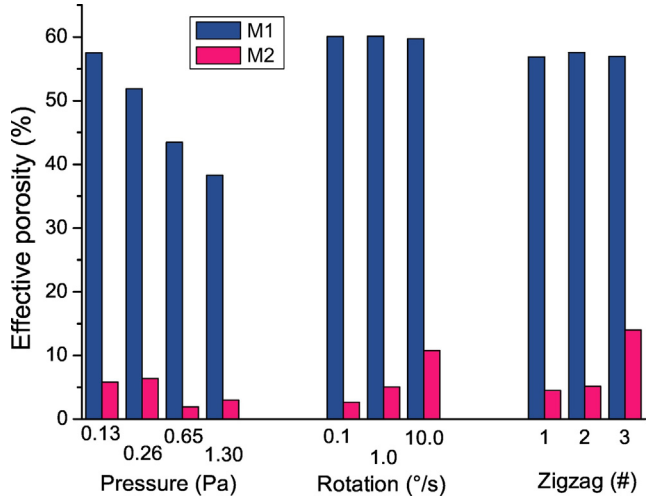

Fig. 21. kMC 3D analysis of the porosity for different film morphologies with pore sizes above 0.64 nm (M1) and 3.2 nm (M2).

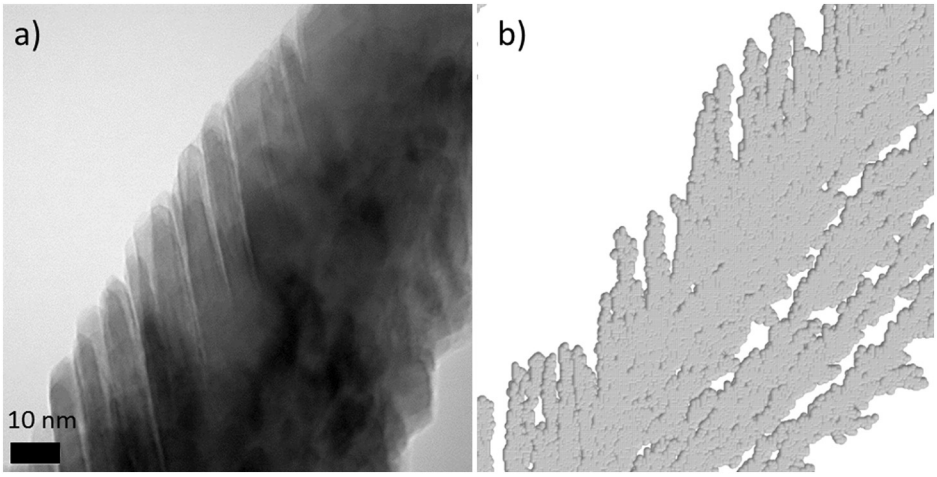

Fig. 22. TEM image of a Ti micro column constituted by nanocolumns from a Ti thin film synthesized at $P = 0.13$ Pa, $P = 150$ W and $\alpha = 85°$ (a) and the corresponding simulation where each atom is represented by its covalent radius (b).

scales. During the growth, the transitions between the nano/micro/macro column structures occur as a function of the film thickness. Upon increase of the film thickness, the nanocolumns agglomerate to form larger micro column structures. Consequently, when using low-mobility deposition conditions, the film morphology generally consists of columnar structures with an intricate, hierarchical structure. In this condition, the specific surface area values evaluated by Brunauer-Emmett-Teller theory comprise also the porosity from nanocolumns, which is not available for the grafting of molecules with a large size. Nevertheless, this structure, which systematically spans a wide range of characteristic dimensions from few to hundreds of nanometers, is very well described by the NASCAM simulation. We can consider that NASCAM can be used to obtain a very good description of the film structure from nano to macro scale and could be used to evaluate Φ_e.

Then, the result reveals that: (i) an increase of the sputtering pressure induces a decrease of Φ_e likely associated with the decrease of the inter-columnar space occurring, leading to the densification of the film and (ii) a high rotation speed or a high number of zigzags during the deposition lead to the largest Φ_e value. The latter behavior could be explained by the high density of early-growing columns, which stop rising after the orientation of the substrate (with respect to the sputter target plane) is modified. A reduced number of growing columns leads to an increase of the inter-columnar space. It appears also that the value of Φ_e associated with the M1 molecule is less influenced by the modification of the φ angle. This is likely associated with the significantly smaller size of this molecule, which allows it to impregnate the film even without φ angle variation. This means that an increase of the pore size (by φ angle modification) has no influence on the associated Φ_e values.

4. Conclusions

In a first attempt, we have set up the deposition parameters allowing the growth of nanostructured thin films using glancing angle magnetron sputtering (MS-GLAD). The effects of the different parameters such as the angle of deposition (α), the substrate temperature or the working pressure on the thin film morphology were studied. Based on this set of data and thanks to the support of kinetic Monte Carlo (kMC) simulation, a better insight into the growth mechanisms of these films using MS-GLAD.

The increase of α leads to the nanostructuration of the films in the form of highly porous structures composed by well separated tilted columns. The lower columnar tilt angle (β) value in comparison to α was explained by the parallel momentum conservation which induces an adatom diffusion in the direction given by the vapor beam sputtered on the film surface. Furthermore, the similar morphology of the thin films synthesized at extreme grazing angle (from $\alpha = 85°$ to 89°) was explained by the geometric inclination of the substrate leading to an asymmetric deposition which consequently increases the deviation angle of incident particles (>10°).

A decrease of the columnar tilt angle when increasing the pressure was explained by the collimation of the incident particle flux. The increase of the collision probability is mainly dependent on the mean free path of the sputtered Ti atoms which is inversely proportional to the sputtering pressure. The mean free path was lower than the distance between the target and the substrate (8 cm) for a pressure value around 0.7 Pa. Below this pressure, very few collisions occurring through the vapor phase were calculated (0.7 at 0.13 Pa) whereas a higher pressure led to numerous collisions between particles (25 at 1.3 Pa). The modification of trajectories is well depicted by the angular and energy distribution calculated for the incoming Ti atoms at the substrate. These data demonstrate that the main processes defining the microstructure of these films are (i) the self-shadowing mechanisms at the surface and (ii) the collisional processes of the sputtered particles in the gas phase.

At low temperature conditions, negligible surface diffusion occur since β is still constant for both the simulations carried out with and without diffusion. In this case, the energy brought to the growing film was too low compared to the energy of Ti self-diffusion process. However, for higher T_s (>523 K), the self-diffusion starts to affect the film morphology and lower β values were observed (from 52.7° at 373 K to 41.2 at 873 K). It can be explained by considering the effect of the surface diffusion of Ti adatoms combined with the effect of the conservation of the parallel momentum. This combination leads to an anisotropic surface diffusion promoting the hops in the direction of incident particles and thus the decrease of β. As previously shown, the parallel momentum affects β and this effect is enhanced by a high diffusion as, under oblique incidence, the diffusion is considerably larger.

For all conditions, the kMC simulations data nicely support the experimental observations even for complex structures such as pillar or zigzag morphologies. This indicates that the simulations realistically reproduce i) the ballistic deposition processes leading to the shadowing effect, ii) the self-diffusion of the adatoms and iii) the competitive growth mechanism involved in the GLAD experiments. By this joint experimental and modeling study, we got a better understanding of the main mechanisms governing the growth of porous Ti coatings synthesized by MS-GLAD. This will allow to finely control the morphology of porous Ti thin film.

Moreover, the NASCAM simulations were used to calculate the roughness and the effective porosity (Φ_e) of the structures. From a

general perspective, analyzing the roughness and the porosity (effective, open, closed, total) evaluated from simulations for any thin film morphologies might be of interest, whatever the applications.

Acknowledgements

The authors would like to thank the "Fédération Wallonie-Bruxelles" through the ARC project MADSSCELLS (AUWB-2012-12/17-UMONS No. 2), the Science Policy Office of the Belgian Federal Government through the "Pôle d'Attraction Interuniversitaire" program (PAI, P7/34, "Plasma-Surface Interaction", Ψ and PAI 7/5 'Functional Supramolecular Systems') and FNRS-FRFC. Dr Mireille RICHARD-PLOUET and Stéphane Grolleau from Institut des Matériaux Jean Rouxel de Nantes (IMN) for the porosity measurements. SK is research associate of National Fund for Scientific Research (FNRS – Belgium).

References

[1] M. Hawkeye, M. Taschuk, M. Brett, Glancing Angle Deposition of Thin Films: Engineering the Nanoscale, John Wiley & Sons, Ltd., Chichester, UK, 2014.
[2] D.W. Flaherty, Z. Dohn'alek, Dohn'alkov, Reactive ballistic deposition of porous TiO_2 films: growth and characterization, J. Phys. Chem. C 111 (2007) 4765–4773.
[3] J.J. Steele, M.J. Brett, Nanostructure engineering in porous columnar thin films: recent advances, J. Mater. Sci. Mater. Electron. 18 (2007) 367–379.
[4] K.M. Krause, M.T. Taschuk, K.D. Harris, D.A. Rider, N.G. Wakefield, J.C. Sit, J.M. Buriak, M. Thommes, M.J. Brett, Surface area characterization of obliquely deposited metal oxide nanostructured thin films, Langmuir 26 (2010) 4368–4376.
[5] J. Dervaux, P.-A. Cormier, S. Konstantinidis, R. Di Ciuccio, O. Coulembier, P. Dubois, R. Snyders, Deposition of porous titanium oxide thin films as anode material for dye sensitized solar cells, Vacuum 114 (2014) 213–220.
[6] S. Lucas, P. Moskovkin, Simulation at high temperature of atomic deposition, islands coalescence, Ostwald and inverse Ostwald ripening with a general simple kinetic Monte Carlo code, Thin Solid Films 518 (2010) 5355–5361.
[7] NASCAM, http://www.unamur.be/sciences/physique/pmr/telechargement/logiciels/nascam.
[8] V. Godinho, P. Moskovkin, R. Álvarez, J. Caballero-Hernández, R. Schierholz, B. Bera, J. Demarche, A. Palmero, A. Fernández, S. Lucas, On the formation of the porous structure in nanostructured a-Si coatings deposited by dc magnetron sputtering at oblique angles, Nanotechnology 25 (2014) 355705.
[9] A.B. Bortz, M.H. Kalos, J.L. Lebowitz, A new algorithm for Monte Carlo simulation of Ising spin systems, J. Comput. Phys. 17 (1975) 10–18.
[10] C.H. Claassens, M.J.H. Hoffman, J.J. Terblans, H.C. Swart, Kinetic Monte Carlo simulation of the growth of various nanostructures through atomic and cluster deposition: application to gold nanostructure growth on graphite, J. Phys. Conf. Ser. 29 (2006) 185–189.
[11] P. Meakin, J. Krug, Three-dimensional ballistic deposition at oblique incidence, Phys. Rev. A 46 (1992) 3390–3399.
[12] T. Smy, D. Vick, M.J. Brett, S.K. Dew, A.T. Wu, J.C. Sit, K.D. Harris, Three-dimensional simulation of film microstructure produced by glancing angle deposition, J. Vac. Sci. Technol. A 18 (2000) 2507.
[13] J.F. Ziegler, M.D. Ziegler, J.P. Biersack, SRIM – the stopping and range of ions in matter (2010), Nucl. Instrum. Methods Phys. Res., Sect. B 268 (2010) 1818–1823.
[14] K.V. Aeken, SIMTRA, www.draft.ugent.be.
[15] J.C. Sit, D. Vick, K. Robbie, M.J. Brett, Thin film microstructure control using glancing angle deposition by sputtering, J. Mater. Res. 14 (1999) 1197–1199.
[16] Z. Li, L. Xing, N. Zhang, Y. Yang, Z. Zhang, Preparation and photocatalytic property of TiO_2 columnar nanostructure films, Mater. Trans. 52 (2011) 1939–1942.
[17] L. Abelmann, C. Lodder, Oblique evaporation and surface diffusion, Thin Solid Films 305 (1997) 1–21.
[18] S. Dew, T. Smy, M. Brett, Step coverage, uniformity and composition studies using integrated vapour transport and film-deposition models, Jpn. J. Appl. Phys. 33 (1994) 1140–1145.
[19] M.M. Hawkeye, M.J. Brett, Glancing angle deposition: fabrication, properties, and applications of micro- and nanostructured thin films, J. Vac. Sci. Technol. A 25 (2007) 1317.
[20] D. Vick, T. Smy, M.J. Brett, Growth behavior of evaporated porous thin films, J. Mater. Res. 17 (2011) 2904–2911.
[21] James William Rohlf, Modern physics from aα to Z0, Mod. Phys. (1994).
[22] R. Alvarez, J.M. Garcia-Martin, M.C. Lopez-Santos, V. Rico, F.J. Ferrer, J. Cotrino, A.R. Gonzalez-Elipe, A. Palmero, On the deposition rates of magnetron sputtered thin films at oblique angles, Plasma Process. Polym. 11 (2014) 571–576.
[23] A. Palmero, H. Rudolph, F.H.P.M. Habraken, One-dimensional analysis of the rate of plasma-assisted sputter deposition, J. Appl. Phys. 101 (2007) 83307.
[24] J.M. García-Martín, R. Alvarez, P. Romero-Gómez, A. Cebollada, A. Palmero, Tilt angle control of nanocolumns grown by glancing angle sputtering at variable argon pressures, Appl. Phys. Lett. 97 (2010) 173103.
[25] R. Alvarez, J.M. Garcia-Martin, A. Garcia-Valenzuela, M. Macias-Montero, F.J. Ferrer, J. Santiso, V. Rico, J. Cotrino, A.R. Gonzalez-Elipe, A. Palmero, Nanostructured Ti thin films by magnetron sputtering at oblique angles, J. Phys. D. Appl. Phys. 49 (2016) 45303.
[26] P.-A. Cormier, A.-L. Thomann, V. Dolique, A. Balhamri, R. Dussart, N. Semmar, T. Lecas, P. Brault, R. Snyders, S. Konstantinidis, IR emission from the target during plasma magnetron sputter deposition, Thin Solid Films 545 (2013) 44–49.
[27] I. Petrov, P.B. Barna, L. Hultman, J.E. Greene, Microstructural evolution during film growth, J. Vac. Sci. Technol. A 21 (2003) S117.
[28] B.A. Movchan, A.V. Demchishin, Structure and properties of thick condensates of nickel, titanium, tungsten, aluminium oxides, and zirconium dioxide in vacuum, Fiz. Met. Metalloved. 28 (1969) 653–660.
[29] J.A. Thornton, The microstructure of sputter-deposited coatings, J. Vac. Sci. Technol. A 4 (1986) 3059–3065.
[30] P. Barna, M. Adamik, Fundamental structure forming phenomena of polycrystalline films and the structure zone models, Thin Solid Films 317 (1998) 27–33.
[31] B.A. Movchan, A.V. Demchishin, Structure and properties of thick condensates of nickel, titanium, tungsten, aluminium oxides, and zirconium dioxide in vacuum, Fiz. Met. Metalloved. 28 (1969) 653–660.
[32] R.N. Tait, T. Smy, M.J. Brett, Modelling and characterization of columnar growth in evaporated films, Thin Solid Films 226 (1993) 196–201.
[33] A. Siad, A. Besnard, C. Nouveau, P. Jacquet, Critical angles in DC magnetron glad thin films, Vacuum 131 (2016) 305–311.
[34] J. Askill, Tracer Diffusion Data for Metals, Alloys, and Simple Oxides, IFI/Plenum Data Corporation, New York, Washington, London, 1970.
[35] J.M. Blocher, I.E. Campbell, Vapor pressure of titanium, J. Am. Chem. Soc. 71 (1949) 4040–4042.
[36] B. Dick, M.J. Brett, T. Smy, Controlled growth of periodic pillars by glancing angle deposition, J. Vac. Sci. Technol., B: Microelectron. Nanometer Struct.–Process., Meas., Phenom. 21 (2003) 23.
[37] D. Le Bellac, G.A. Niklasson, C.G. Granqvist, Scaling of surface roughness in obliquely sputtered chromium films, Europhys. Lett. 32 (1995) 155–159.
[38] A. Dolatshahi-Pirouz, M.B. Hovgaard, K. Rechendorff, J. Chevallier, M. Foss, F. Besenbacher, Scaling behavior of the surface roughness of platinum films grown by oblique angle deposition, Phys. Rev. B 77 (2008) 115427.
[39] K. Rechendorff, M.B. Hovgaard, J. Chevallier, M. Foss, F. Besenbacher, Tantalum films with well-controlled roughness grown by oblique incidence deposition, Appl. Phys. Lett. 87 (2005) 73105.
[40] R. Álvarez, L. González-García, P. Romero-Gómez, V. Rico, J. Cotrino, A.R. González-Elipe, A. Palmero, Theoretical and experimental characterization of TiO_2 thin films deposited at oblique angles, J. Phys. D. Appl. Phys. 44 (2011) 385302.
[41] C. Buzea, K. Kaminska, G. Beydaghyan, T. Brown, C. Elliott, C. Dean, K. Robbie, Thickness and density evaluation for nanostructured thin films by glancing angle deposition, J. Vac. Sci. Technol., B: Microelectron. Nanometer Struct.–Process., Meas., Phenom. 23 (2005) 2545.
[42] T. Karabacak, J.P. Singh, Y.-P. Zhao, G.-C. Wang, T.-M. Lu, Scaling during shadowing growth of isolated nanocolumns, Phys. Rev. B 68 (2003) 125408.
[43] K.M. Krause, M. Thommes, M.J. Brett, Pore analysis of obliquely deposited nanostructures by krypton gas adsorption at 87K, Microporous Mesoporous Mater. 143 (2011) 166–173.
[44] PORESTAT, Available from: http://nanoscops.icmse.csic.es/software/porestat.
[45] R. Messier, Revised structure zone model for thin film physical structure, J. Vac. Sci. Technol. A 2 (1984) 500.